Research Article

Im-Fong Ip, Yi-Shan Wang, and Chia-Chen Chang*

Aptamer-based detection of serotonin based on the rapid *in situ* synthesis of colorimetric gold nanoparticles

https://doi.org/10.1515/ntrev-2022-0514
received July 13, 2022; accepted January 11, 2023

Abstract: Serotonin, a neurotransmitter that affects brain function, is associated with cancer progression, thus making it a potential biomarker. Despite the increasing efforts and ideas for gold nanoparticle (AuNP)-based colorimetric detection over the years, preparing AuNPs and sensing targets are separate processes, and this incurs more time to operate and produces excess waste. Herein, we report a simple, sensitive, and rapid colorimetric detection method for serotonin based on the *in situ* formation of AuNP. When only the aptamer is present, it can prevent chloride-induced aggregation of AuNPs because it easily binds to the freshly synthesized AuNPs through its exposed bases to increase the positive charge of the AuNP surfaces. When a complex of serotonin and its aptamer is formed, this complex disturbs the adsorption between aptamers and AuNPs, resulting in reduced stability of AuNPs and easy aggregation of nanoparticles. Therefore, serotonin was measured by color change, consistent with the change in peak intensity in the UV-vis absorption spectrum. The sensor demonstrated good sensitivity with a detection limit of 1 ng/mL (5.7 nM) for serotonin, which is comparable to or better than that of other aptamer-based colorimetric detection methods, further exhibiting the requisite selectivity against possible interferents. These results serve as a basis for developing other biosensors using aptamer-mediated *in situ* growth of AuNPs.

Keywords: *in situ* formation, gold nanoparticle, colorimetric assay, aptamer, serotonin detection

*** Corresponding author: Chia-Chen Chang,** Department of Medical Biotechnology and Laboratory Science, Chang Gung University, Taoyuan 333, Taiwan; Department of Nephrology, Chang Gung Memorial Hospital, Kidney Research Center, Taoyuan 333, Taiwan, e-mail: chang@cgu.edu.tw
Im-Fong Ip, Yi-Shan Wang: Department of Medical Biotechnology and Laboratory Science, Chang Gung University, Taoyuan 333, Taiwan

1 Introduction

Serotonin is a neurotransmitter found in many different organs throughout the human body, including the brain, lungs, kidneys, and gastrointestinal tract [1]. It has been recently discovered that serotonin is a positive regulator of tumors, implying that there is a causal relationship between serotonin concentration in blood and disease [2]. Therefore, determining these serotonin molecules in biological samples is crucial for disease surveillance and development of new treatment medicines.

Various methods have been developed to detect serotonin. Electrochemical methods for detecting redox reactions have been widely used to construct biosensors for serotonin because these neurotransmitters are generated *via* oxidative metabolism [3–5]. However, to achieve high selectivity for serotonin, these approaches can be challenging because the oxidation potentials of related nonspecific biomolecules are often quite similar, making it hard to identify them from electrical signals [6]. Other reported methods for detecting serotonin include fluorescence [7], high-performance liquid chromatography [8], and capillary electrophoresis [9]. These methods are time-consuming and labor-intensive and require expensive equipment and tedious sample preparation, limiting their application to real samples [10–15]. Furthermore, antibodies are used as probes in the majority of methods to capture target molecules. However, the antibodies are limited by their ease of deactivation and instability, resulting in the divergence of the measured target values between different assays [16–18]. The aptamer has a high affinity for its target and a number of noteworthy features such as design flexibility, ease of synthesis, and specificity [19,20]. Therefore, alternative assays that use aptamers have been developed.

Gold nanoparticle (AuNP)-based assays are an interesting and attractive strategy for developing biosensing probes because of their unique properties [21–25]. Godoy-Reyes *et al.* developed a colorimetric sensor for serotonin

based on chemical molecular recognition [26]. Chávez *et al.* proposed aptamer-modified AuNPs for the colorimetric detection of serotonin [27]. Although these AuNP-based approaches are selective, these two assays require the pre-synthesis of AuNPs and modification of molecular probes on AuNPs, requiring additional time, effort, and resources. Therefore, a simple, quick, and sensitive method for determining serotonin levels is urgently needed.

Herein, we developed a convenient platform for the rapid detection of serotonin during *in situ* AuNP formation based on different levels of aptamers and aptamer–target complexes resistant to chloride-induced AuNP aggregation. AuNPs formed with aptamers have seldom been reported, even though the AuNPs formed *in situ* have been used in different chemical sensor applications [28,29]. Different properties of AuNP aggregates can be used to determine the amount of serotonin in a solution. As shown in Scheme 1, without the aptamer and its target, AuNPs can be formed by reducing the gold ions with ascorbic acid and stabilized by adsorbed unreacted positive Au ions whose repulsion prevents the van der Waals attraction between AuNPs from aggregation. After introducing the NaCl solution, additional chloride ions are coordinated to the gold ions on the surface of the AuNPs, which has a negative effect on the electrostatic stabilization of the formed AuNPs [30–32], causing the AuNPs to self-aggregate and causing the color to change from red to blue. In the presence of the aptamer alone, the phosphate backbones of the single-stranded DNA (ssDNA) aptamer can interact with unreacted gold ions owing to electrostatic adsorption, while the exposed bases in the ssDNA aptamer can be spontaneously adsorbed to the *in situ* synthesized AuNPs, thus stabilizing the AuNPs and demonstrating a red color. Nevertheless, the binding between the aptamer and AuNPs is disturbed in the presence of serotonin and its aptamer because serotonin recognizes and binds its aptamer. As a result, the same mechanism is not operative with the ssDNA aptamer/serotonin complex because the folded aptamer structure does not permit the uncoiling required to expose the bases. AuNPs easily become unstable when chloride ions are added to the solution, leading to their aggregation. Generally, it is convenient to detect serotonin molecules using the naked eye; thus, the proposed aptamer detection strategy that integrates the *in situ* rapid formation of AuNPs will be of great interest.

2 Experimental section

2.1 Chemicals

Chloroauric acid ($HAuCl_4$), ascorbic acid, serotonin, epinephrine, dopamine, acetylcholine, 10× phosphate-buffered saline, and 50× Tris-acetate EDTA (TAE) were obtained from Sigma-Aldrich (St. Louis, MO, USA). Human plasma (Type AB), used for practical application tests, was purchased from Sigma-Aldrich. Quant-iT OliGreen ssDNA reagent was obtained from Thermo Fisher (Eugene, OR, USA). The serotonin ELISA kit was from Lifespan Biosciences (Seattle, WA, USA). All solutions were prepared using Milli-Q deionized water with a resistivity of 18.2 M/m

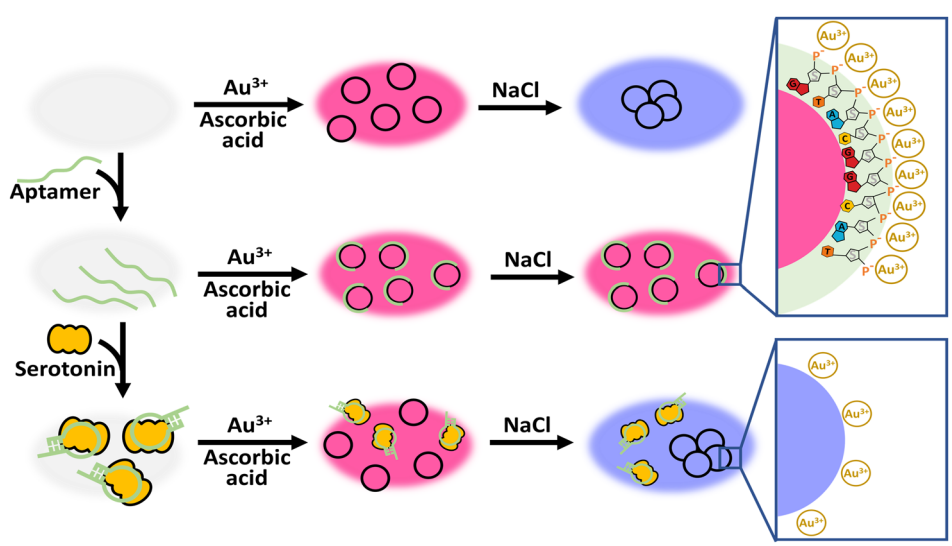

Scheme 1: Schematic representation of the aptamer-based colorimetric assay for the colorimetric detection of serotonin molecules *via in situ* synthesis of AuNPs.

(Millipore, Billerica, MA). All the research images were captured using iPhone 11 (Apple, Cupertino, CA, USA). Oligonucleotides normalized to 100 μM in TAE buffer were purchased from Purigo Biotech (Taipei, Taiwan). The aptamer sequence used was as follows: CGACTGGTAGGCAGATAGGG GAAGCTGATTCGATGCGTGGGTCG [33].

2.2 Colorimetric detection of serotonin

One microliter of 100 μM anti-serotonin aptamer and 1 μL of different serotonin concentrations were added to 1× TAE buffer (solution A). Subsequently, 50 μL of solution A was incubated at 30°C for 30 min. Next, 1 μL of solution A was mixed with 33 μL of 1 mM $HAuCl_4$, and the volume of this solution was adjusted to 95 μL by adding deionized water (solution B). Then, 5 μL of 100 mM ascorbic acid was quickly added to solution B and mixed evenly at room temperature for 20 s, producing a red color immediately owing to the formation of AuNPs. After 5 min, 1 μL 4 M NaCl was added to the AuNP solution for 10 min reaction. Finally, absorbance was measured using a SpectraMax iD3 microplate reader (Molecular Devices, San Jose, CA, USA). The spectra were measured with a resolution of 5 nm over a wavelength range of 400–800 nm. All measurements were performed in sterile 96-well plates for a total volume of 100 μL.

3 Results and discussion

3.1 Characterization of synthesized AuNPs

As shown in Figure 1a, aqueous $HAuCl_4$ solution was reduced by ascorbic acid under different conditions. Upon reduction, all solutions appeared ruby red (inset of Figure 1a). The UV-

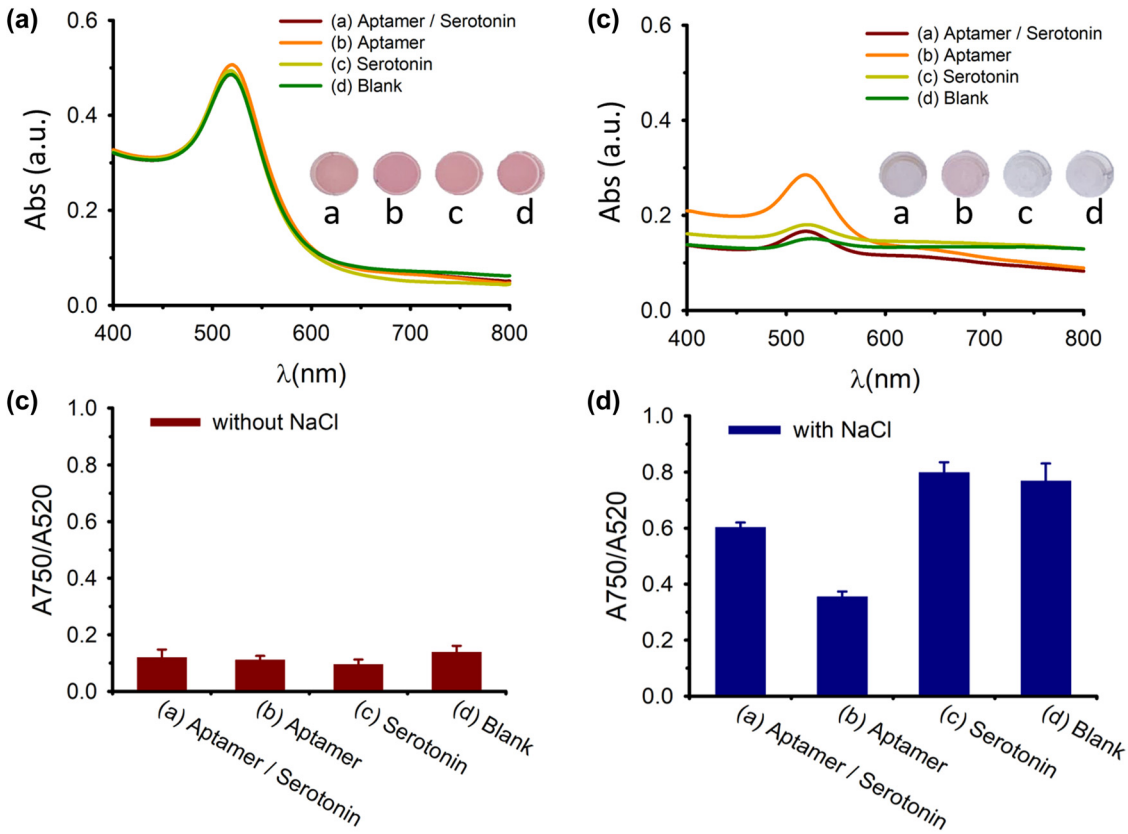

Figure 1: UV-Vis absorption spectra of the colorimetric assay in the different conditions (a) with and (b) without adding NaCl. Inset shows the images of the color change of the AuNP solution. The ratio of the absorbance at 750 and 520 nm of the AuNP solution (c) with and (d) without adding NaCl in the presence of (a) aptamer and serotonin, (b) aptamer, (c) serotonin, and (d) blank. The final concentrations of aptamer, serotonin, and NaCl were 20 nM, 10 ng/mL, and 32 mM, respectively, and their pH was 4. The error bars represent the standard deviation of the mean of three measurements (for the representation of the curves in this figure in color, the reader is referred to view the web version of this article).

visible spectra of these solutions showed the same characteristic peak at 520 nm. Transmission electron microscopy (TEM) images of the synthesized AuNPs are shown in Figure S1. The spherical nanoparticles could be clearly observed, and the average diameters determined from the TEM images were approximately 17–20 nm, which was consistent with the surface plasmon resonance (SPR) band at approximately 520 nm [34]. The time course of the absorption signal responses was recorded to investigate the stability of these AuNPs. The synthesized AuNPs stabilized by DNA aptamers are shown in Figure S2, which remained stable for over 15 h. Contrastingly, the stability of AuNPs without aptamers could only be maintained for 7.5 h. The presence of oligonucleotides provided a certain degree of stability to the formed AuNPs. When salt ions were added, different spectra and color changes were observed in different solutions. When only reduced AuNPs were present in the solution (Figure 1b(d)), the absorbance signal at 520 nm sharply decreased, and that at a long wavelength of approximately 700 nm increased, accompanied by a color change from red to blue. Similar responses were observed in the presence of serotonin and reduced AuNPs (Figure 1b(c)). After the addition of aptamer (Figure 1b(b)), although the absorbance intensity at 520 nm decreased from 0.5 to 0.3, the color was still reddish, indicating that the aptamer protects the reduced AuNPs from the salt-induced aggregation reaction. In contrast, the absorbance of the reaction solution containing the aptamer and serotonin molecules (Figure 1b(a)) was ~2-fold higher at 520 nm than that without serotonin. To estimate the degree of AuNP aggregation, the absorption ratio of 750 and 520 nm ($A750/A520$) as an aggregation parameter was determined; a higher ratio value indicates a stronger degree of aggregation. As shown in Figure 1c, all values of the absorption ratio were less than 0.2, indicating the dispersion of the reduced AuNPs without NaCl. When salt ions were added (Figure 1d), the absorption ratio of the aptamer alone was substantially lower than that of the blank group, while that of serotonin alone

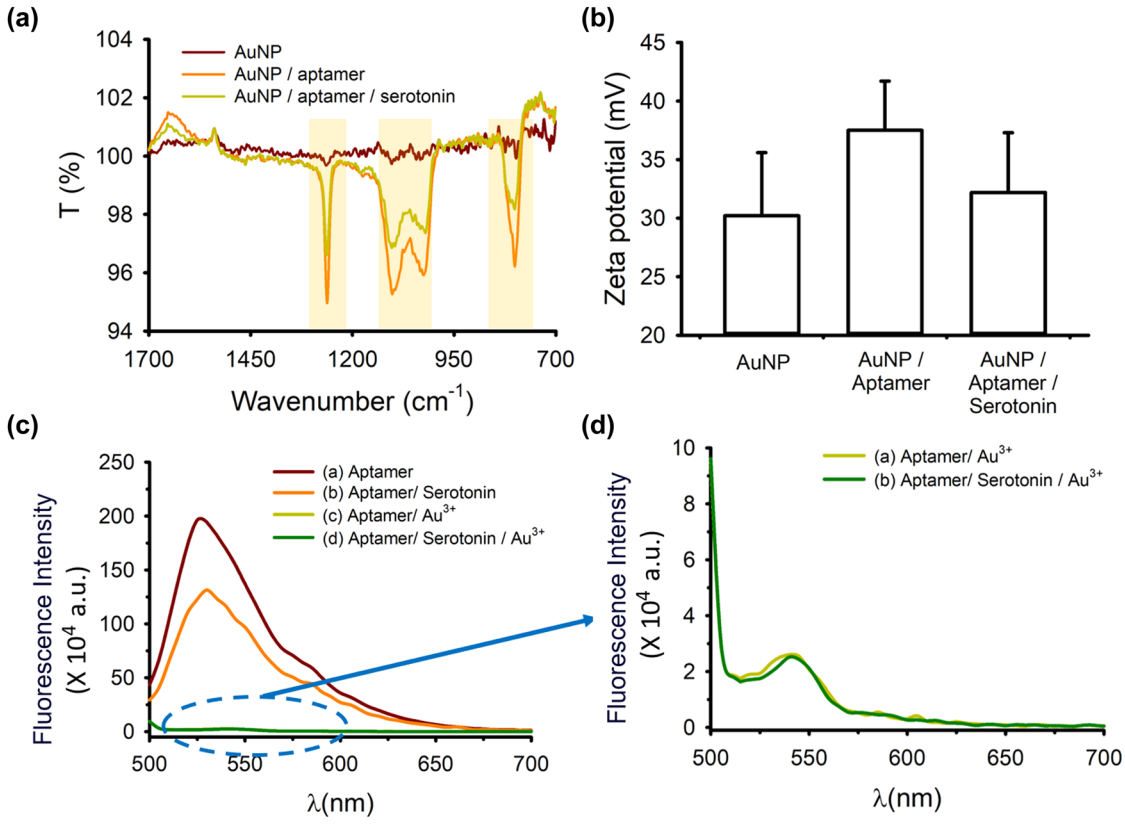

Figure 2: (a) FTIR and (b) zeta potential responses of synthesized AuNPs only, AuNPs with DNA aptamer, and AuNPs with DNA aptamer and serotonin. The final concentrations of aptamer, serotonin, and NaCl were 20 nM, 10 ng/mL, and 32 mM, respectively. (c) Fluorescence spectra of the Oligreen with aptamer only, aptamer/serotonin complex, aptamer and gold ion, and aptamer/serotonin complex and gold ion. (d) Magnified view of the fluorescence spectra of the Oligreen with aptamer and gold ion, and aptamer/serotonin complex and gold ion. The error bars represent the standard deviation of the mean of three measurements (For the representation of the curves in this figure in color, the reader is referred to view the web version of this article.).

was nearly identical to that of the control group, implying that while serotonin has no effect on reduced AuNPs, the aptamer has a role in preventing the aggregation of AuNPs. The absorption ratio was larger when both aptamer and serotonin were present than when the aptamer existed alone, indicating that the binding of serotonin to its aptamer would limit the attachment of the aptamer to AuNPs.

To better understand the mechanism of AuNP formation, FTIR spectroscopy was used to probe the interactions among the DNA aptamer, serotonin, and the reduced AuNPs (Figure 2a). The dips at 802, 1,025, 1,101, and 1,262 cm^{-1} were attributed to the vibrations of the sugar phosphate [35], deoxyribose [36], phosphate [37], and phosphodiester bonds [38] of nucleic acids, respectively. Thus, several changes at these wavenumbers could be observed in the presence of the aptamer and reduced AuNPs, indicating interactions between the aptamer and AuNPs. When the aptamer was first mixed with serotonin, the four dips were significantly weakened. In this case, a portion of the aptamers did not interact with the AuNPs because of complex formation between the aptamer and serotonin. The zeta potential was used to determine the surface charge of the synthesized AuNPs in solution. As shown in Figure 2b, the positive zeta potential of the AuNPs indicated the presence of positively charged surface ligands, probably leaving unreacted Au ions. The Oligreen ssDNA fluorescence assay was used to prove the interaction between DNA aptamers and gold ions [39,40]. Figure 2c illustrates that when Oligreen interacted with each ssDNA aptamer in the presence and absence of targets, brighter fluorescence resulted from the Oligreen interaction with the aptamer alone than with the aptamer/serotonin complex, which is consistent with the previous Oligreen study [40]. When gold ions were added, a remarkable decrease in fluorescence intensity was observed in the presence of the aptamer and aptamer/serotonin complex (Figure 2d), implying that fluorescent oligo green molecules were detached from DNA owing to the interaction between the aptamer and gold ions. Additionally, in the presence of gold ions, the decrease in fluorescence with only aptamer was higher than that with the aptamer/serotonin complex. This indicates that gold ions interact more favorably with the ssDNA aptamer than the complex of the aptamer and serotonin; thus, the aptamer alone is easier to adsorb quickly on the reduced AuNPs. Therefore, these results demonstrate that the solution with aptamers stabilized the ascorbic acid-synthesized AuNPs against aggregation at salt concentrations that ordinarily screen the repulsive

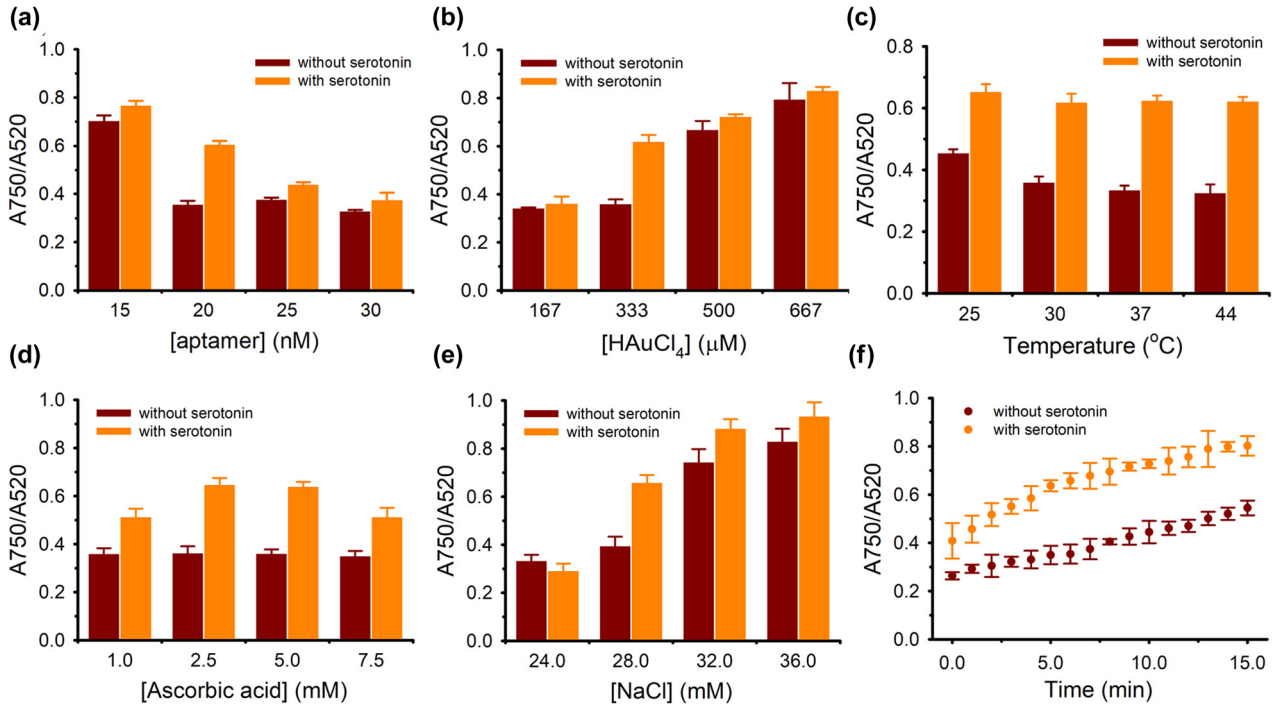

Figure 3: Effect of different condition parameters on the spectral responses with *in situ* prepared AuNPs in the presence and absence of 10 ng/mL serotonin: (a) aptamer concentration, (b) gold ion concentration, (c) reaction temperature, (d) ascorbic acid concentration, (e) NaCl concentration, and (f) the reaction time after the addition of NaCl. The error bars represent the standard deviation of the mean of three measurements.

interactions of the unreacted gold ions, whereas the solution with aptamer/serotonin complexes did not provide stability to the synthesized AuNPs, and the solution turned blue. Thus, based on the color changes caused by the rapid *in situ* synthesis of AuNPs, the target molecule levels could be directly observed, facilitating the detection of serotonin in a simple and convenient manner.

3.2 Optimization of the experimental conditions

Several experimental parameters of this colorimetric method were optimized to maximize assay performance, including the concentrations of the aptamer, gold ions, ascorbic acid, and NaCl, the incubation time, and the experimental temperature. As shown in Figure 3a, with increasing aptamer concentration, the absorption ratio decreased with and without serotonin. Furthermore, more aptamers could prevent AuNP from salt-induced aggregation, but they also caused fewer changes in the signal response when serotonin was present. To achieve a better detection response, 20 nM aptamer was chosen as the optimal condition. The concentration of $HAuCl_4$ ions had a significant impact on the growth of AuNPs. Interestingly, when the concentration of $HAuCl_4$ ions was 333 μM, the absorption ratio was significantly different in the presence and absence of serotonin (Figure 3b). A low concentration of $HAuCl_4$ ions may produce fewer AuNPs; thus, the aptamer can effectively protect AuNPs from salt-induced aggregation and vice versa. Therefore, 333 μM $HAuCl_4$ ions was deemed optimal and used for the following measurements. Moreover, the assay performance of the colorimetric behavior was influenced by the reaction temperature in the interaction of aptamers and targets. The absorption ratio increased progressively from 25 to 30°C, and there were no significant differences ($p > 0.05$) when the temperature was increased to 44°C (Figure 3c). Therefore, we optimized the temperature to 30°C. Subsequently, a series of different concentrations of ascorbic acid and sodium chloride were optimized. Figure 3d and e exhibited that ascorbic acid of 2.5 mM and sodium chloride of 28 mM were selected to obtain the optimal response. Finally, the response time after the addition of NaCl was explored, and 5 min was used in subsequent experiments (Figure 2f). The experimental ranges and optimum conditions for the test parameters are summarized in Table S1.

3.3 Detection of serotonin

After optimizing the experimental conditions, we examined the response to serotonin. Before adding salt, the absorption spectra of the AuNP solutions remained nearly unchanged with different concentrations of serotonin molecules; thus, the color also appeared red (Figure S3),

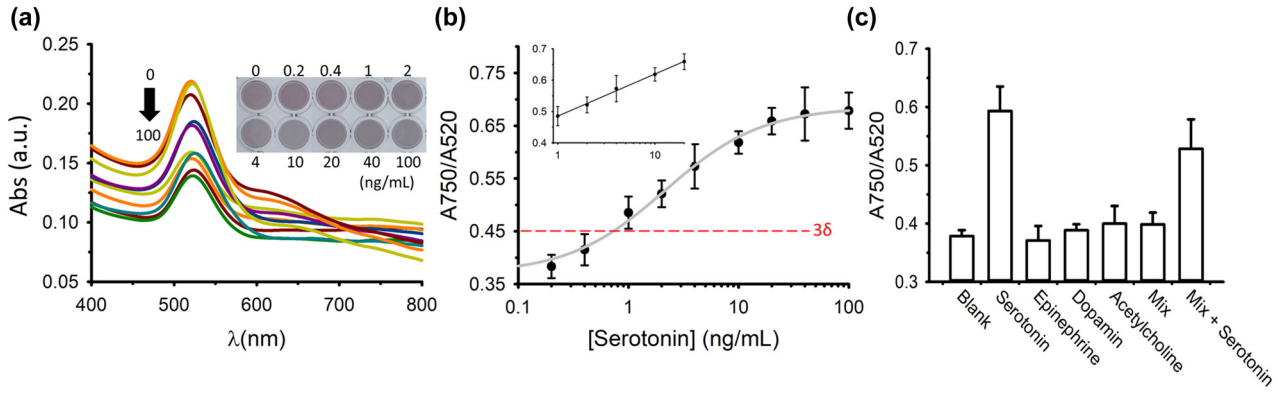

Figure 4: Sensing performance of the colorimetric AuNPs for serotonin. (a) Absorption spectra of the AuNP solution at various serotonin concentrations. The inset shows the image of the AuNP solution containing different concentrations of serotonin. (b) Calibration plot of serotonin using the ratio of the absorbance at 750 and 520 nm of the AuNP solution at various serotonin concentrations. "3σ" is drawn at the zero-dose value plus thrice the standard deviation of the zero-dose measurements. The linear relationship was observed at the serotonin concentration from 1 to 20 ng/mL (R^2 = 0.997 in the inset). The final concentrations of aptamer, Au^{3+}, ascorbic acid, and NaCl were 20 nM, 333 μM, 2.5 mM, and 28 mM, respectively, and their pH was 4. (c) Absorbance ratio in the presence of related interfering molecules at 20 ng/mL. The concentration of serotonin used in the specificity was 10 ng/mL. Mix represents the reaction solution containing all the interference molecules except for serotonin at 20 ng/mL. The error bars represent the standard deviation of the mean of three measurements (for the representation of the curves in this figure in color, the reader is referred to view the web version of this article).

Table 1: Comparison of the performance on serotonin detection between our method and other previous assays

Detection method	Working range	LOD (nM)	Sensing material preparation	Signal response time (min)	Practical application	Ref.
Colorimetric (aptamer-capped AuNP)	0.8–2.5 μM	300	Moderate	12	Fetal bovine serum	[26]
Colorimetric (dithiobis succinimidylpropionate and *N*-acetyl-L-cysteine-modified AuNPs)	0–3 μM	120	Moderate	9	Simulated serum	[27]
Colorimetric (dimeric-serotonin bivalent ligand-modified AuNPs)	100–300 nM	2.6	Moderate	6	Diluted human serum	[41]
Electrochemical (FeC-AuNPs-MWCNT-modified screen-printed carbon electrode)	0.1–20 μM	17	Complex	2.5	Artificial urine	[42]
Electrochemical (gold nanoflowers modified carbon fiber microelectrode)	1–100 μM	300	Moderate	30	Artificial cerebrospinal fluid	[43]
Electrochemical (rGO-Ag_2Se/GCE)	0.1–15 μM	29.6	Moderate	3	0.1% Human serum	[44]
Electrochemical (Ni NPs-rGO/GCE)	0.1–2 μM	10	Moderate	—	10% Human urine	[45]
Fluorescence (QDs@SiO_2@MIPs)	0.3–2.8 μM (50–500 ng/mL)	3.9 (0.69 ng/mL)	Complex	11	2.5% Human serum	[46]
FETs (ZnO nanorod)	0.1 fM to 1 nM	0.1 fM	Complex	20	Diluted human serum	[47]
Colorimetric (aptamer-capped *in situ* synthesized AuNP)	5.7–114 nM (1–20 ng/mL)	5.7 (1 ng/mL)	Simple	5	0.5% Human serum	Our work

GCE, glass carbon electrode; MWCNT, multi-walled carbon nanotube; rGO, reduced graphene oxide; QD, quantum dots; SiO_2, silica nanoparticle; MIP, molecularly imprinted polymer.

Table 2: Recovery test for serotonin detection in real samples

Samples	Added (ng/mL)	Found by our assay (ng/mL) $n = 3$	Measured by ELISA (ng/mL) $n = 3$	Recovery (%)	RSD (%)
Diluted serum	1	1.1 ± 0.1	1 ± 0.2	110	8.8
	2	1.8 ± 0.2	2.3 ± 0.4	90	12.7
	10	10.2 ± 1.5	10.5 ± 0.9	102	14.0
	20	18.3 ± 1.9	22.4 ± 2.3	91.5	10.2

indicating that serotonin did not have a significant effect on the formation of AuNPs. In the presence of salt, the qualitative results can be observed with the naked eye, and the colloid solution color changed from red to dark red or even dark purple-blue (inset of Figure 4a). Quantitative results were obtained from changes in the optical spectra (Figure 4a). When the experimental data were fitted to the calibration curve with four-parameter logistic regression, the correlation coefficient (R^2) was 0.991, indicating satisfactory agreement (Figure 4b). With an increase in the serotonin concentration, the absorption intensity at 520 nm continued to decrease, while that at 750 nm continued to increase. The scatter plot shown in the inset of Figure 4b showed the relationship between the $A750/A520$ values and serotonin concentrations. A good linear relationship with R^2 of 0.997 was obtained between the $A750/A520$ ratio and the logarithm of serotonin concentration in the range of 1–20 ng/mL. The limit of detection (LOD) of this assay was 1 ng/mL (corresponding to 5.7 nM using a molecular weight of 176 g/mol of serotonin), based on three times the standard deviation of the control. As shown in Table 1, the LOD of our assay was comparable or superior to those of colorimetric detection using pre-synthesized AuNPs [26,27,41], electrochemical assays based on different nanomaterial-modified electrodes [42–45], and Mn^{2+}-doped ZnS quantum dot (QD)-modified fluorescence sensors based on molecularly imprinted polymers [46]. Although this assay demonstrated a lower LOD than the zinc oxide (ZnO) nanorod-based field-effect transistor (FET) for the detection of serotonin [47], our method has the advantage of easy preparation. Therefore, the preparation using our colorimetric assay could be performed faster than that with ZnO-based FET, incurring a long time (over 24 h) and high temperature (350°C) of FET chip fabrication. Furthermore, compared with previously described analytical assays as well as other gold nanomaterial-based colorimetric methods, our approach is distinguished by its speed and simplicity. Notably, our assay required less than 1 min to prepare, which was considerably less than almost all previous approaches.

Furthermore, we investigated the selectivity of our assay by adding various interfering species at a concentration of 20 ng/mL (Figure 4c). The addition of these species with similar chemical structures did not cause an obvious variation in the absorption ratio values. To further verify the selectivity for the practical detection of serotonin, coexisting interfering species and their mixtures with twice the amount of serotonin were examined. A relatively higher absorption ratio was obtained in the solution mixture spiked with 10 ng/mL serotonin than in the solution without serotonin. This result revealed that the current approach is capable of selecting serotonin with the appropriate selectivity.

As one step further toward actual human body fluid measurement, we challenged our assay with serotonin spiking and concentration recovery experiments in blood samples. We started with 50- to 500-fold diluted serum samples that were not spiked with serotonin. As shown in Figure S4, the response for nonspecific binding decreased from 200-fold dilution onward, with identical values for 500-fold dilution. Solutions from serum samples (200-fold dilution) were spiked with an increasing number of serotonin standards. The concentrations were also determined by a validated spectrophotometric method using the ELISA kit. Table 2 shows that the average serotonin recoveries varied from 90 to 110%, with relative standard deviations (RSDs) ranging from 8.8 to 14.0%. In addition, there was a good agreement between the colorimetric assay we used and that determined by the validated method in the serum samples. These results indicate that the developed method has the potential to identify and detect the target serotonin in real samples. In this study, the LOD was determined to be 1 ng/mL in the pure buffer system, but the samples were diluted 200 times before measurement in practical applications. Thus, it can be estimated that the LOD for the undiluted serum sample was 200 ng/mL or higher. For practical applications, greater efforts are required to increase the LOD of this detection approach by utilizing more sensitive detectors (such as SPR sensors) [48,49] or adding antifouling materials [50,51].

4 Conclusions

In this study, a simple colorimetric biosensor for detecting serotonin was developed in the rapid synthesis of AuNPs.

At room temperature, the formation of AuNPs was accomplished using ascorbic acid as the reducer of Au^{3+} without adding any other capping agents. The assay was based on the different adsorption properties of the aptamer and aptamer/serotonin complex toward the synthesized AuNPs owing to their electrostatic properties. Our proposed method has advantages in addition to its simplicity, cost-effectiveness, and rapid analysis. Moreover, our LOD, as low as 1 ng/mL (5.7 nM), is comparable to or better than that in reported assays for serotonin. More importantly, our sensing strategy does not require a pre-synthesis step of AuNPs, making the process less laborious. In view of these features, we expect that this detection strategy may offer the potential to detect a wide spectrum of analytes when used properly.

Acknowledgments: The authors thank the Microscopy Center at Chang Gung University for technical assistance and the manuscript was edited by Editage.

Funding information: This work was supported by Ministry of Science and Technology of Taiwan (109-2113-M-182-004-MY2 and 111-2221-E-182-017).

Author contributions: I.I.: conceptualization, methodology, and writing – original draft preparation; I.I. and Y.W.: formal analysis and investigation; C.C.: supervision and writing – review and editing; C.C.: project administration; C.C.: funding acquisition. All authors have accepted responsibility for the entire content of this manuscript and approved its submission.

Conflict of interest: The authors state no conflict of interest.

Data availability statement: The datasets generated during and/or analysed during the current study are available from the corresponding author on reasonable request.

References

[1] Scotton WJ, Hill LJ, Williams AC, Barnes NM. Serotonin syndrome: pathophysiology, clinical features, management, and potential future directions. Int J Pharmtech Res. 2019;12:1–14.
[2] Sarrouilhe D, Mesnil M. Serotonin and human cancer: a critical view. Biochimie. 2019;161:46–50.
[3] Sharma S, Singh N, Tomar V, Chandra R. A review on electrochemical detection of serotonin based on surface modified electrodes. Biosens Bioelectron. 2018;107:76–93.
[4] Khoshnevisan K, Honarvarfard E, Torabi F, Maleki H, Baharifar H, Faridbod F, et al. Electrochemical detection of serotonin: a new approach. Clin Chim Acta. 2020;501:112–9.
[5] Movassaghi CS, Perrotta KA, Yang H, Iyer R, Cheng X, Dagher M, et al. Simultaneous serotonin and dopamine monitoring across timescales by rapid pulse voltammetry with partial least squares regression. Anal Bioanal Chem. 2021;413(27):6747–67.
[6] Nishitani S, Sakata T. Enhancement of signal-to-noise ratio for serotonin detection with well-designed nanofilter-coated potentiometric electrochemical biosensor. ACS Appl Mater Interfaces. 2020;12(13):14761–9.
[7] Kim Y, Kim J. Synthesis of carbon dots *via* hydrothermal reaction for selective detection of serotonin. J Nanosci Nanotechnol. 2020;20(9):5365–8.
[8] Islam J, Shirakawa H, Nguyen TK, Aso H, Komai M. Simultaneous analysis of serotonin, tryptophan and tryptamine levels in common fresh fruits and vegetables in Japan using fluorescence HPLC. Food Biosci. 2016;13:56–9.
[9] Roychoudhury A, Francis KA, Patel J, Jha SK, Basu S. A decoupler-free simple paper microchip capillary electrophoresis device for simultaneous detection of dopamine, epinephrine and serotonin. RSC Adv. 2020;10(43):25487–95.
[10] Fazlali F, Hashemi P, Khoshfetrat SM, Halabian R, Baradaran B, Johari-Ahar M, et al. Electrochemiluminescent biosensor for ultrasensitive detection of lymphoma at the early stage using CD20 markers as B cell-specific antigens. Bioelectrochemistry. 2021;138:107730.
[11] Hashemi P, Afkhami A, Bagheri H, Amidi S, Madrakian T. Fabrication of a novel impedimetric sensor based on l-Cysteine/Cu(II) modified gold electrode for sensitive determination of ampyra. Anal Chim Acta. 2017;984:185–92.
[12] Khanmohammadi A, Jalili Ghazizadeh A, Hashemi P, Afkhami A, Arduini F, Bagheri H. An overview to electrochemical biosensors and sensors for the detection of environmental contaminants. J Iran Chem Soc. 2020;17(10):2429–47.
[13] Khoshfetrat SM, Bagheri H, Mehrgardi MA. Visual electrochemiluminescence biosensing of aflatoxin M1 based on luminol-functionalized, silver nanoparticle-decorated graphene oxide. Biosens Bioelectron. 2018;100:382–8.
[14] Bordbar MM, Samadinia H, Sheini A, Aboonajmi J, Javid M, Sharghi H, et al. Non-invasive detection of COVID-19 using a microfluidic-based colorimetric sensor array sensitive to urinary metabolites. Microchim Acta. 2022;189(9):1–11.
[15] Parvin S, Hashemi P, Afkhami A, Ghanei M, Bagheri H. Simultaneous determination of BoNT/A and/E using an electrochemical sandwich immunoassay based on the nanomagnetic immunosensing platform. Chemosphere. 2022;298:134358.
[16] Arshavsky-Graham S, Urmann K, Salama R, Massad-Ivanir N, Walter JG, Scheper T, et al. Aptamers *vs* antibodies as capture probes in optical porous silicon biosensors. Analyst. 2020;145(14):4991–5003.
[17] Lopez-Silva C, Surapaneni A, Coresh J, Reiser J, Parikh CR, Obeid W, et al. Comparison of aptamer-based and antibody-based assays for protein quantification in chronic kidney disease. Clin J Am Soc Nephrol. 2022;17(3):350–60.
[18] Chang CC. Recent advancements in aptamer-based surface plasmon resonance biosensing strategies. Biosensors. 2021;11(7):233.
[19] Saito S. SELEX-based DNA aptamer selection: a perspective from the advancement of separation techniques. Anal Sci. 2021;37(1):17–26.

[20] Chang CC, Yeh CY. Using simple-structured split aptamer for gold nanoparticle-based colorimetric detection of estradiol. Anal Sci. 2021;37(3):479–84.
[21] Stobiecka M, Deeb J, Hepel M. Ligand exchange effects in gold nanoparticle assembly induced by oxidative stress biomarkers: homocysteine and cysteine. Biophys Chem. 2010;146:98–107.
[22] Stobiecka M, Coopersmith K, Hepel M. Resonance elastic light scattering (RELS) spectroscopy of fast non-Langmuirian ligand-exchange in glutathione-induced gold nanoparticle assembly. J Colloid Interface Sci. 2010;350:168–77.
[23] Hepel M, Blake D, McCabe M, Stobiecka M, Coopersmith K. Assembly of gold nanoparticles induced by metal ions. In Functional nanoparticles for bioanalysis, nanomedicine, and bioelectronic devices. Vol. 1, Washington DC, USA: American Chemical Society; 2012. p. 207–40.
[24] He Z, Yin H, Chang CC, Wang G, Liang X. Interfacing DNA with gold nanoparticles for heavy metal detection. Biosensors. 2020;10(11):167.
[25] Li CF, Yang ZH, Lin PY, Chang HC, Yang CW, Chang CC. Target-induced recycling assembly of split aptamer fragments by DNA toehold-mediated displacement for the amplified colorimetric detection of estradiol. Sens Actuators B Chem. 2020;364:131823.
[26] Godoy-Reyes TM, Llopis-Lorente A, Costero AM, Sancenón F, Gaviña P, Martínez-Máñez R. Selective and sensitive colorimetric detection of the neurotransmitter serotonin based on the aggregation of bifunctionalised gold nanoparticles. Sens Actuators B Chem. 2018;258:829–35.
[27] Chávez JL, Hagen JA, Kelley-Loughnane N. Fast and selective plasmonic serotonin detection with aptamer-gold nanoparticle conjugates. Sensors. 2017;17(4):681.
[28] Tang S, Tong P, Lu W, Chen J, Yan Z, Zhang L. A novel label-free electrochemical sensor for Hg^{2+} based on the catalytic formation of metal nanoparticle. Biosens Bioelectron. 2014;59:1–5.
[29] Lv P, Zhou H, Mensah A, Feng Q, Wang D, Hu X, et al. A highly flexible self-powered biosensor for glucose detection by epitaxial deposition of gold nanoparticles on conductive bacterial cellulose. Chem Eng J. 2018;351:177–88.
[30] Luty-Błocho M, Wojnicki M, Fitzner K. Gold nanoparticles formation *via* Au(III) complex ions reduction with l-ascorbic acid. Int J Chem Kinet. 2017;49(11):789–97.
[31] Luty-Błocho M, Wojnicki M, Grzonka J, Kurzydłowski KJ, Fitzner K. Linking the gold nanoparticles formation kinetics with their morphology. Int J Chem Kinet. 2018;50(3):204–14.
[32] Walters DT, Aghakhanpour RB, Powers XB, Ghiassi KB, Olmstead MM, Balch AL. Utilization of a nonemissive triphosphine ligand to construct a luminescent gold(I)-box that undergoes mechanochromic collapse into a helical complex. J Am Chem Soc. 2018;140(24):7533–42.
[33] Nakatsuka N, Faillétaz A, Eggemann D, Forró C, Vörös J, Momotenko D. Aptamer conformational change enables serotonin biosensing with nanopipettes. Anal Chem. 2021;93(8):4033–41.
[34] Sun Y, Xia Y. Gold and silver nanoparticles: a class of chromophores with colors tunable in the range from 400 to 750 nm. Analyst. 2003;128(6):686–91.
[35] Kelly JG, Martin-Hirsch PL, Martin FL. Discrimination of base differences in oligonucleotides using mid-infrared spectroscopy and multivariate analysis. Anal Chem. 2009;81(13):5314–9.
[36] Pięta E, Petibois C, Pogoda K, Suchy K, Liberda D, Wróbel TP, et al. Assessment of cellular response to drug/nanoparticles conjugates treatment through FTIR imaging and PLS regression study. Sens Actuators B Chem. 2020;313:128039.
[37] Hârţa M, Borsai O, Muntean CM, Dina NE, Fălămaş A, Olar LE, et al. Assessment of genetic relationships between *Streptocarpus* x *hybridus* V. parents and F1 progenies using SRAP markers and FT-IR spectroscopy. Plants. 2020;9(2):160.
[38] Tang Y, Wei W, Liu Y, Liu S. Fluorescent assay of FEN1 activity with nicking enzyme-assisted signal amplification based on ZIF-8 for imaging in living cells. Anal Chem. 2021;93(11):4960–6.
[39] Bruno JG, Sivils JC. Studies of DNA aptamer OliGreen and PicoGreen fluorescence interactions in buffer and serum. J Fluoresc. 2016;26(4):1479–87.
[40] Huang CC, Chang HT. Aptamer-based fluorescence sensor for rapid detection of potassium ions in urine. Chem Commun. 2008;12:1461–3.
[41] Chavan SG, Yagati AK, Kim HT, Jin E, Park SR, Patil DV, et al. Dimeric-serotonin bivalent ligands induced gold nanoparticle aggregation for highly sensitive and selective serotonin biosensor. Biosens Bioelectron. 2021;191:113447.
[42] Wu B, Yeasmin S, Liu Y, Cheng LJ. Sensitive and selective electrochemical sensor for serotonin detection based on ferrocene-gold nanoparticles decorated multiwall carbon nanotubes. Sens Actuators B Chem. 2022;354:131216.
[43] Li R, Li X, Su L, Qi H, Yue X, Qi H. Label-free electrochemical aptasensor for the determination of serotonin. Electroanalysis. 2022;34(6):1048–53.
[44] Panneer Selvam S, Yun K. A self-assembled silver chalcogenide electrochemical sensor based on rGO-Ag_2Se for highly selective detection of serotonin. Sens Actuators B Chem. 2020;302:127161.
[45] Ran G, Xia Y, Liang L, Fu C. Enhanced response of sensor on serotonin using nickel-reduced graphene oxide by atomic layer deposition. Bioelectrochemistry. 2021;140:107820.
[46] Wang Z, Zhang Y, Zhang B, Lu X. Mn^{2+} doped ZnS QDs modified fluorescence sensor based on molecularly imprinted polymer/sol–gel chemistry for detection of serotonin. Talanta. 2018;190:1–8.
[47] Sinha K, Chakraborty B, Chaudhury SS, Chaudhuri CR, Chattopadhyay SK, Mukhopadhyay CD. Selective, ultra-sensitive, and rapid detection of serotonin by optimized ZnO nanorod FET biosensor. IEEE Trans NanoBioscience. 2022;21(1):65–74.
[48] Yang CH, Wu TH, Chang CC, Lo HY, Liu HW, Huang NT, et al. Biosensing amplification by hybridization chain reaction on phase-sensitive surface plasmon resonance. Biosensors. 2021;11(3):75.
[49] Wu TH, Yang CH, Chang CC, Liu HW, Yang CY, Shen TL, et al. Multi-layer reflectivity calculation based meta-modeling of the phase mapping function for highly reproducible surface plasmon resonance biosensing. Biosensors. 2021;11(3):95.
[50] Cui M, Ma Y, Wang L, Wang Y, Wang S, Luo X. Antifouling sensors based on peptides for biomarker detection. Trends Anal Chem. 2020;127:115903.
[51] Wu J, Zhao C, Hu R, Lin W, Wang Q, Zhao J, et al. Probing the weak interaction of proteins with neutral and zwitterionic antifouling polymers. Acta Biomater. 2014;10(2):751–60.